NANO LETTERS

pubs.acs.org/NanoLett

Near UV LEDs Made with in Situ Doped p-n Homojunction ZnO Nanowire Arrays

Min-Teng Chen,[†,∥] Ming-Pei Lu,[‡,∥] Yi-Jen Wu,[†] Jinhui Song,[§] Chung-Yang Lee,[†] Ming-Yen Lu,[†] Yu-Cheng Chang,[†] Li-Jen Chou,[†] Zhong Lin Wang,[§] and Lih-Juann Chen*[,†]

[†]Department of Materials Science and Engineering, National Tsing Hua University, Hsinchu, Taiwan 30043 Republic of China, [‡]National Nano Device Laboratories, Hsinchu, Taiwan 30078, Republic of China, and [§]School of Materials Science and Engineering, Georgia Institute of Technology, Atlanta, Georgia 30332, United States

ABSTRACT Catalyst-free p-n homojunction ZnO nanowire (NW) arrays in which the phosphorus (P) and zinc (Zn) served as p- and n-type dopants, respectively, have been synthesized for the first time by a controlled in situ doping process for fabricating efficient ultraviolet light-emitting devices. The doping transition region defined as the width for P atoms gradually occupying Zn sites along the growth direction can be narrowed down to sub-50 nm. The cathodoluminescence emission peak at 340 nm emitted from n-type ZnO:Zn NW arrays is likely due to the Burstein−Moss effect in the high electron carrier concentration regime. Further, the electroluminescence spectra from the p-n ZnO NW arrays distinctively exhibit the short-wavelength emission at 342 nm and the blue shift from 342 to 325 nm is observed as the operating voltage further increasing. The ZnO NW p-n homojunctions comprising p-type segment with high electron concentration are promising building blocks for short-wavelength lighting device and photoelectronics.

KEYWORDS ZnO nanowires, p-n homojunction, Near UV LED, in situ doped

The short-wavelength photoelectronics devices, such as ultraviolet light-emitting diodes (UV LEDs) and ultraviolet laser diodes (UV LDs), have attracted tremendous attention for the widely used applications in the fields of the long-lifetime displays, the illumination devices, UV photolithography, the high-density information storage and biomedical sensors.[1−9] Among those wide-bandgap semiconductor materials such as ZnO, GaN, AlN, and other III−V and II−VI compounds, ZnO is the most promising candidate for use as functional building blocks in the efficient UV LEDs due to its large bandgap of 3.37 eV and the high exciton binding energy of 60 meV. The UV emissions from ZnO homojunctions comprising the p- and n-type ZnO layers serving as hole and electron injection layers, respectively, had been reported previously.[6,10,11] However, p-type ZnO materials are difficult to be realized due to the self-compensation mechanism involving oxygen vacancies and zinc interstitials and the low solubility of dopants, compared to the as-grown ZnO naturally exhibiting n-type characteristics.[12,13] Recently, the nanowire-based LEDs have been of great interest for the possibility to integrate UV photoelectronic NW devices into the high-density functional nanochips. So far, only a few reports are available about the fabrication of the ZnO nanowires (NWs) with the p-n homojunctions, in which p-type dopants were introduced by ion implantation[14,16] and thermal diffusion process[15] to create the hole injection segments. However, the p-type doping profiles of p-n homojunctions synthesized by those two ex-situ doping approaches cannot be precisely controlled with high spatial resolution and would increase integration complications, implying that it will limit the practical applications of the p-n ZnO NWs, especially for use in integrated photoelectric circuits.

In this letter, we report the synthesis of the catalyst-free epitaxial p-n homojunction ZnO NW arrays in which the phosphorus (P) -doped and zinc (Zn) -doped ZnO act as p- and n-type segments, respectively, with a sub-50 nm doping transition region created by the in situ doping process. The cathodoluminescence (CL) emission peak at 340 nm from ZnO/Zn NW arrays is observed, which is associated with the high electron carrier concentration. The electroluminescence (EL) spectra indicated that the shortest wavelength of light emitted from p-n ZnO NW arrays is 325 nm under the high operating voltage. Moreover, the narrow-width doping transition region in this p-n ZnO NWs can presumably result in the blue shift in short-wavelength light emitted from n-type segments.

The ZnO p-n NW arrays were grown on n-type Si (001) wafers with thin ZnO films on the top by using a thermal vapor deposition method without growth catalysts[17,18] in a three-zone furnace. The zinc phosphate (Zn_3P_2) powders served as the P dopant source to fabricate the p-type ZnO segment. The Zn_3P_2 powders and the mixture of ZnO and graphite powders were placed in alumina boats and positioned at the first and second zones of the furnace at 350 and 1050 °C, respectively. The ZnO-coated Si substrates, fabricated from the Si substrate covered with zinc acetate

* To whom correspondence should be addressed. E-mail: ljchen@mx.nthu.edu.tw.
∥ Authors with equal contributions.
Received for review: 05/30/2010
Published on Web: 00/00/0000

© XXXX American Chemical Society

DOI: 10.1021/nl101907h | *Nano Lett.* **XXXX,** *xxx,* 000–000

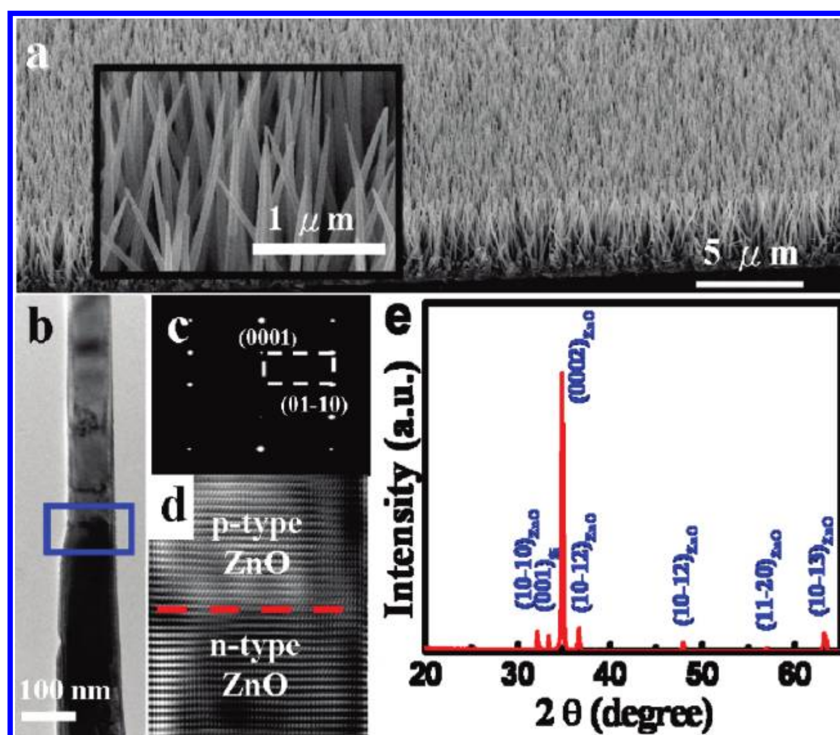

FIGURE 1. Morphological and structural characterization of the p-n ZnO NW arrays. (a) Low-magnification SEM image of the vertically aligned p-n ZnO NW arrays grown on ZnO-coated Si substrate. High-magnification SEM image of the p-n ZnO NW arrays showing gradually tapered NWs in the inset figure. (b) The low-magnification TEM image of a single ZnO NW comprising the n- and p-type segments. (c) The selected area electron diffraction pattern (SAED) with the [0001] growth direction. (d) High-resolution TEM image of the region around the p-type ZnO (top)/n-type ZnO (bottom) interface showing the high-quality epitaxial growth without any transition phase. (e) XRD spectrum of the p-n ZnO NW arrays observed without any peaks associated with other phases.

thin films through the annealing process at 390 °C in air, were positioned horizontally inside the tube furnace at a pressure of 1.0×10^{-3} Torr. A carrier gas of 100 sccm Ar and 10 sccm O_2 were kept with the constant flow rate. The growth temperature was maintained at 600 °C and the pressure inside the growth furnace was fixed at 1 Torr. Prior to the introduction of the doping gas to synthesize the p-type segment of p-n ZnO NWs, the ZnO:Zn NW arrays regarded as the n-type segment were grown vertically on the ZnO-coated Si substrates. Importantly, the p-type segment would be epitaxially grown on the top of the n-type ZnO NWs, showing the aligned p-n ZnO NWs in this continuous growth process.

Figure 1a shows a low-magnification SEM image of the vertically aligned p-n ZnO NW arrays. The length of the p-n ZnO NWs was measured to be in the range of 4−5 μm. The high-magnification SEM image depicted in the inset of Figure 1a demonstrates the side view morphology of the ZnO:P NW segment, which shows the gradually tapered structure at the top of the p-type segment similar to the P doped nanostructures reported previously.[19] In addition, the P atoms are uniformly distributed in the p-type segment of the ZnO NWs along radial direction rather than only incorporated into the surface region of NW (see Figure S1 in Supporting Information). The low-magnification transmission electron microscopy (TEM) image of a single ZnO NW comprising the n- and p-type segments is shown in Figure 1b. The interface between the two segments is enclosed by the solid blue-square as presented in the figure. The selected area electron diffraction (SAED) pattern recorded from a single p-n ZnO NW reveals that the entire NW is of single-crystal nanostructure grown in [0001] direction of wurtzite ZnO structure (Figure 1c). A high-resolution transmission electron microscopy (HRTEM) image including the interface between n- and p-type segments presents clear lattice fringes along the (0001) plane of wurtzite ZnO structure at both side of n- and p-type segments without any transition phase (Figure 1d). It reveals an excellent crystallographic alignment at the p-n interface. An X-ray diffraction (XRD) spectrum of the p-n ZnO NW arrays is shown in Figure 1e. In addition to the (001) peak from the Si substrate, other peaks can all be ascribed to wurtzite ZnO crystal structure, and the relatively strong (0001) peak is consistent with that of TEM observations.

To investigate the doping profile in the p-n ZnO NWs, both the HRTEM images for extracting the lattice spacing and the energy dispersive spectroscopy (EDS) for monitoring the distribution of the Zn, O, and P elements were utilized. The typical high-resolution TEM images recorded from different positions denoted as A-C in Figure 2a are shown in the Supporting Information Figure S2. The traces of the lattice spacing and the EDS profile with respect to the relative position along the growth direction are presented in Figure 2. The lattice spacing trace (upper panel of Figure 2) dem-

© XXXX American Chemical Society

DOI: 10.1021/nl101907h | Nano Lett. XXXX, xxx, 000–000

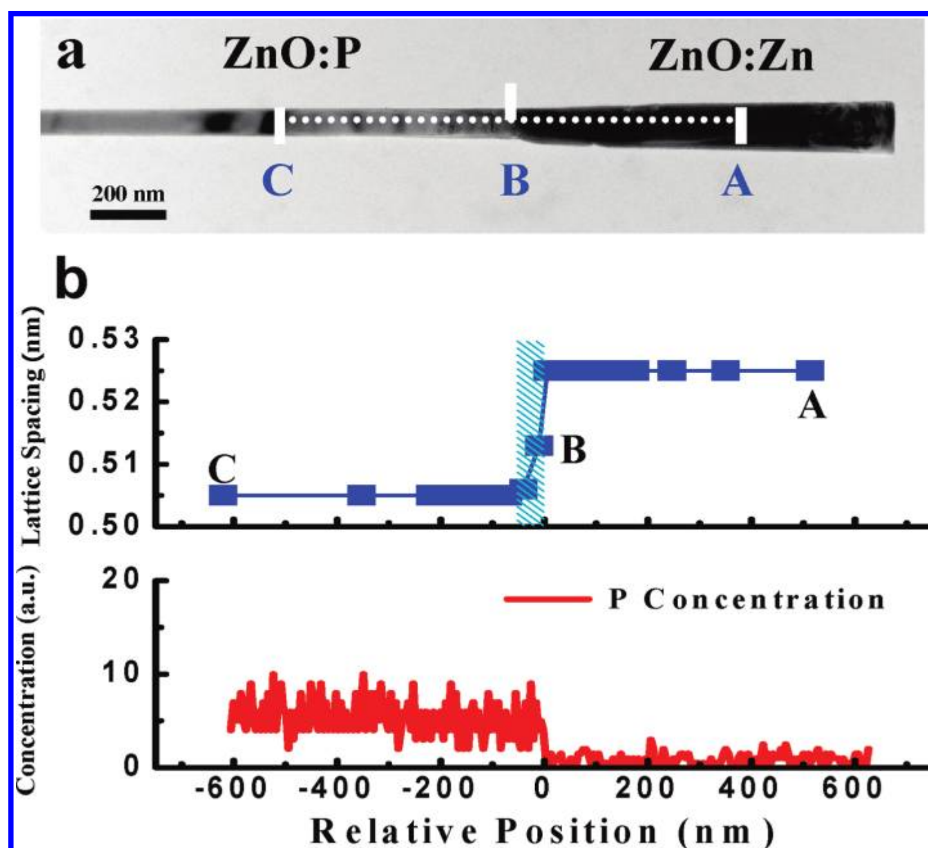

FIGURE 2. The traces of the lattice spacing and the EDS profile along the growth direction from an individual p-n ZnO NW. (a) Low-magnification TEM image of a single p-n ZnO NW. (b) Upper panel: the lattice spacing extracted from n-type segment to p-type segment along the (0001) plane. The doping transition region is marked as the shadow area; bottom panel: the EDS results showing the signals for P element along the growth direction of ZnO NW.

onstrates that the d-spacing corresponding to the (0001) plane of the p-type segments (~0.505 nm) was smaller than that of n-type segment (~0.525 nm) at each regions far away from p-n interface, indicating the formation of $[P_{zn}-2V_{zn}]$ complex serving as acceptor in the P-doped NWs.[13] The P atoms occupying Zn sites would introduce a lattice relaxation due to the significantly shorter bonding length of $P_{zn}-O$ (0.168 nm) than that of Zn−O (0.193 nm), which would result in the reduction of the lattice spacing in p-type segment.[19,20] Significantly, there is a transition region for the lattice spacing changing from 0.525 to 0.505 nm, which is marked with a shadow pattern, at the junction interface as shown in the upper panel of Figure 2b. The EDS results obtained by TEM line-mapping can provide clear information about the relative concentration of P element along the scanned direction as shown in the bottom panel of Figure 2b (the recorded signals of Zn and O elements are not shown here). For spots scanned at the n-type region, elemental signals of Zn and O appeared together without apparent presence of P signals. As the scanned spots crossed the interface of p-n junction and moved further into the p-type region, the elemental signals of P suddenly appear. It is apparent that the doping concentration of the P element in the p-type segment is distributed uniformly not only along the growth direction (Figure 2b) but also in the radial direction (Supporting Information Figure S1). According to the lattice spacing trace as shown in Figure 2b, the decrement of the lattice spacing with respect to the distances from the p-n homojunction interface is observed. It is suggested that the P atoms would gradually occupy Zn sites since the P atoms were started to be introduced into the synthesis process. As a result, the width of the doping transition region, defined as the width for P atoms gradually occupying Zn sites along the growth direction, can be scaled down to sub-50 nm by using the in situ-doping process.

For the purpose of characterizing the electrical property of P-doped ZnO at the upper part of p-n ZnO NW, the piezoelectric measurements were performed at ambient condition to verify the p-type doping characteristics. The piezoelectric properties of the p-n ZnO NWs were measured using a conductive atomic force microscopy (AFM) technique that was demonstrated as a reliable technique for identifying p- and n-type ZnO NW.[20−23] To substantiate the existence of p-type NWs in the current case, the AFM was used to scan across a relatively large area of the sample so that a statistical data can be obtained. In the contact mode, a constant normal force of 80 nN was kept between the AFM tip and NW sample surface. The output voltage across an external resistance (500 MΩ) was continuously recorded when the AFM tip scanned across the p-n NW array with a scanned

© XXXX American Chemical Society

DOI: 10.1021/nl101907h | Nano Lett. XXXX, xxx, 000–-000

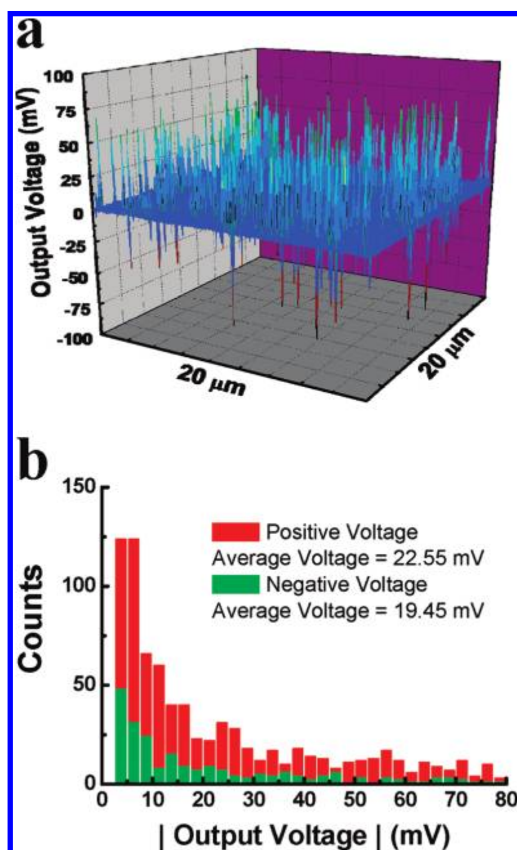

FIGURE 3. Piezoelectric voltage generation using p-n ZnO NWs. (a) Three-dimensional plot of the output voltage pulses recorded simultaneously when conductive AFM tip scanned across the NWs in the contact mode. (b) Statistical distributions of the piezoelectric output voltage recorded from p-n ZnO NWs, indicating the majority of output signal is positive.

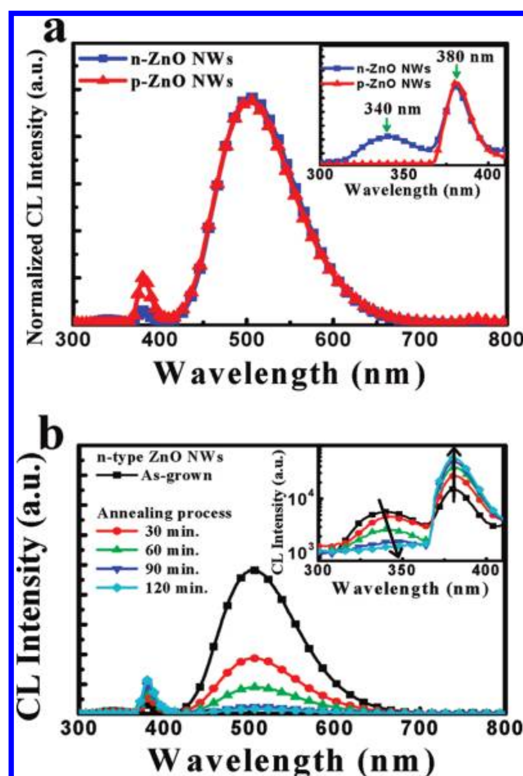

FIGURE 4. (a) Normalized CL spectra of the as-grown n-type and p-type ZnO NW arrays. The enlarged figure of the normalized CL spectra with respect to the wavelength ranging from 300 to 410 nm is shown in the inset. (b) Comparison between the CL spectra of the as-grown n-type NWs and the n-type ZnO NW arrays annealed for various periods of time in the oxygen ambient. The semilogarithmic plot of CL spectra in the wavelength range from 300 to 410 nm is shown in the inset figure.

area of 20 μm × 20 μm. The 3D image of output voltage pulses is shown in Figure 3a, indicating that both positive and negative output voltage pulses can be observed in this case. Note that the positive voltage pulses are much more frequent than that of the negative pulses. The statistical distributions of positive and negative voltage pulses are shown in Figure 3b. The mean value of positive and negative voltage pulses can be calculated as 22.55 and 19.45 mV, respectively. According to previous reports,[20−23] the piezoelectric voltage pulses with positive and negative signs would correspond to the piezoelectric characteristics of p-type and n-type materials, respectively, taking the screening effect of dopants into account. The voltage pulses with negative sign can be presumably contributed by the negative piezoelectric potential inside the n-type NWs. In our case, the diameter of n-type segment is larger than that of p-type segment (see Figure 1b), indicating the AFM tip would probably contact with the n-type segment when the AFM tip scanned across the p-n ZnO NWs. The positive voltage pulses dominated in the piezoelectric measurement would be resulted from the p-type property of P-doped segment at the upper part of p-n ZnO NWs.

The normalized CL spectra of the as-grown n-type and p-type ZnO NW arrays synthesized on the ZnO-coated Si substrates are shown in the Figure 4a. Compared to the CL spectra recorded from the ZnO film-coated Si substrate (Supporting Information Figure S3), the near bandgap emission peak at ∼380 nm and the broad deep-level-related (DL) emission peak at ∼506 nm are evident for both NWs samples. It is obvious that the intensity of DL emission (I_{DL}) exhibits a stronger emission behavior compared to that of UV emission (I_{UV}). Typically, the recombination process contributed by the oxygen-related defects at/near NWs surfaces would play an important role in the contributive proportion of the DL emission.[24−27] As the diameter of NW decreasing, the intensity of DL emission would be enhanced compared to that of UV emission in CL spectra as a result of the surface effect in nanomaterials. In the present study, the diameter of n-type NW (∼90 ± 20 nm) is substantially larger than the depth that defines the effective volume beneath the NW surface which contributes to the surface recombination in CL spectra (typically about 10 nm).[26,27] It suggests that the high density of oxygen-related defects at/near surfaces in ZnO:Zn NWs would give rise to the high I_{DL}/I_{UV} ratio of 16.5 compared to that of ∼1 for n-type NWs with diameter of ∼100 nm.[26] The rough surface morphology in the

© XXXX American Chemical Society

DOI: 10.1021/nl101907h | Nano Lett. XXXX, xxx, 000–000

ZnO:Zn NW giving rise to a high density of surface states is evident in the TEM image, as shown in Supporting Information Figure S4. In addition, the short-wavelength emission at 340 nm is distinctively found in the CL spectra of the n-type ZnO NW arrays. The magnified figure of normalized CL spectra with respect to the wavelength ranging from 300 to 410 nm shows a clear emission peak at 340 nm for n-type ZnO:Zn NW arrays compared to the p-type case as shown in the inset of Figure 4a. To explore the physical mechanism of this short-wavelength CL emission at 340 nm in n-type NWs, annealing in oxygen environment at 600 °C was extended from 30 to 120 min. The inset in the Figure 4b presents the semilogarithmic plot of CL spectrum in the wavelength range from 300 to 410 nm for a comparison. The obvious decrement in I_{DL}/I_{UV} ratio with increasing the oxygen annealing time was attributed to the decrement of oxygen-related defect density in n-type NWs[25] especially near the NW surface. Note that the 340 nm emission in the n-type ZnO NWs would gradually shift to 380 nm and merge into the DL band with increasing annealing time, revealing a correlation between the 340 nm emission peak in CL spectra and the oxygen-related defects in ZnO/Zn NWs. In addition, we also measured the as-grown n-type ZnO nanorod arrays synthesized by an aqueous chemical and downward growth method for the comparison.[28] These samples show not only the typical CL emission spectra comprising UV and DL emission bands without 340 nm emission peak but also the atomic ratio of near 1:1 for both Zn and O, which is similar to that of our samples when exposed to long time oxygen annealing process.

The PL emission peak at 3.55 eV due to quantum confinement effect was previously observed for the ZnO rods with diameter of ∼2 nm that was comparable to the exciton Bohr radius in bulk ZnO.[29] Observation of emission peak at 3.65 eV from ZnO NWs with diameter of 30−40 nm was reported in the literature,[30] suggesting that free carrier confined by the electrical barriers, which were formed in the NWs due to the surface defects or exciton dead layer, contributed to UV emissions. Notably, the thickness of the dead layer at ZnO surface in weak confinement regime is only a few nanometers taking into consideration of the ratio of hole and electron effective masses being 9.5.[31,32] The diameter of our n-type NWs was much larger than the thickness of the dead layer. Therefore, the confinement effect induced by the dead layer at surfaces of ZnO NWs would not take place in our case. It is well-known that the Burstein−Moss (BM) effect, so-called the bandgap widening effect, would take place in the n-type ZnO NWs with high electron carrier concentrations.[33,34] The electron concentration for 340 nm emission in ZnO NWs would be theoretically calculated to be as high as $\sim 10^{20}$ cm^{-3}.[33] The possible physical mechanism for the 340 nm emission is likely related to the high free electron carrier density associated to the high oxygen-related defect density in ZnO:Zn NWs. The electron carrier concentrations in the as-grown n-type NWs can be extracted to be in the range of $0.9-3 \times 10^{18}$ cm^{-3} by using the conventional field-effect method (details in Supporting Information). Importantly, there is a noticeable discrepancy between the extracted carrier concentration and the theoretical electron concentration. On the basis of charge neutrality condition in NWs, the surface depletion width due to surface band bending can be increased linearly with surface state density, which can result in the significant decrement of the effective NW diameter for the NW with high surface defect density.[24] According to our CL results shown in Figure 4a, the high surface defect density as a result of the high I_{DL}/I_{UV} ratio can create the wide surface depletion region in our n-type NWs, indicating the essential carrier concentration in n-type ZnO NWs should be much higher than the extracted value of $0.9-3 \times 10^{18}$ cm^{-3} taking the effective diameter into account. Therefore, the high electron carrier concentration obtained in n-type ZnO:Zn NWs with high oxygen vacancies as well as high zinc interstitial density[35] would be the origin of the 340 nm emission. The observation of 340 nm emission peak in ZnO:Zn NWs can provide promising strategy for use in the short-wavelength optoelectronic applications.

To investigate the electrical characteristics of the p-n ZnO NWs, the two terminal devices were fabricated by using the indium tin oxide (ITO) film as the conducting electrode directly deposited on top of the ZnO NW arrays. Prior to the deposition of ITO film, the poly(methyl methacrylate) (PMMA) film was spin-coated on the NW arrays to prevent the shorting of connection between the top and the bottom electrodes in the two-terminal devices followed by the oxygen plasma treatment to remove the excess PMMA on top of ZnO NWs. The schematic representation of the two-terminal device is illustrated in the inset of Figure 5a. The $I-V$ characteristics of ZnO NW p-n homojunctions were measured in the ambient condition at room temperature as shown in Figure 5a. The electrical characteristics of the NWs present a clear rectifying behavior with the threshold voltage of ∼1 V. In addition, the ohmic and nonlinear electrical behaviors of two-terminal devices were observed for the cases of n-type ZnO NW arrays and p-type NW arrays, respectively. Taking the Schottky barrier (SB) at the interface between ITO and ZnO NWs into account, the SB height for electron injection is lower than that for hole injection due to the ITO work function of 4.7 eV. As a result, the two-terminal electrical characteristics of the p-type NW arrays would exhibit the nonlinear electrical behavior. The semilogarithmic plot of $I-V$ curve measured from p-n ZnO NW arrays is presented in the Figure 5b. The rectification ratios of forward bias to reverse bias current in the p-n homojunction arrays was ∼530 and ∼70 for device operated in the low voltage of ±3 V and the high voltage of ±15 V, respectively.

The EL spectra emitted from the ZnO NW p-n homojunctions with various operating voltages from 35 to 50 V at room temperature are exhibited in Figure 6. The top view photograph of the bright light emitting spot at a driving

© XXXX American Chemical Society

DOI: 10.1021/nl101907h | *Nano Lett.* **XXXX,** *xxx,* 000–000

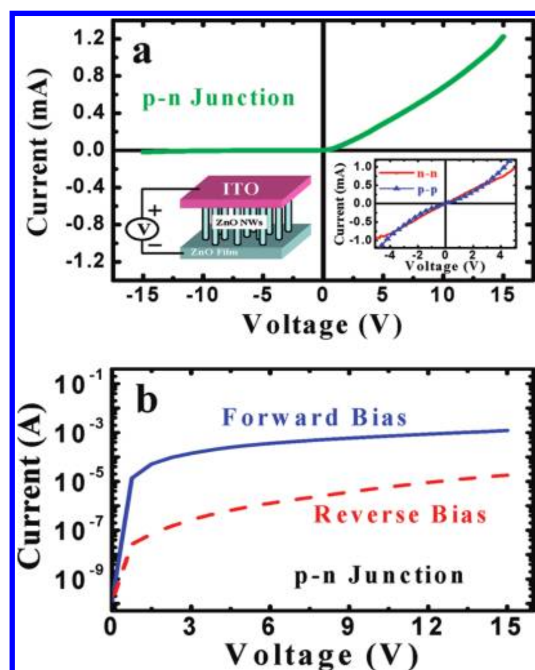

FIGURE 5. $I-V$ characteristics of the p-n ZnO NW arrays at room temperature. (a) The rectifying behavior of two-terminal device comprising the p-n NWs with the threshold voltage of ~1 V. The schematic representation of the two-terminal device is indicated in the bottom-left inset figure. $I-V$ characteristics of n-type and p-type NWs are plotted in the bottom-right inset figure. (b) The semilogarithmic plot of $I-V$ curve of the p-n ZnO NW arrays. The rectification ratio is ~530 for device operated in the low voltage regime of ±3 V.

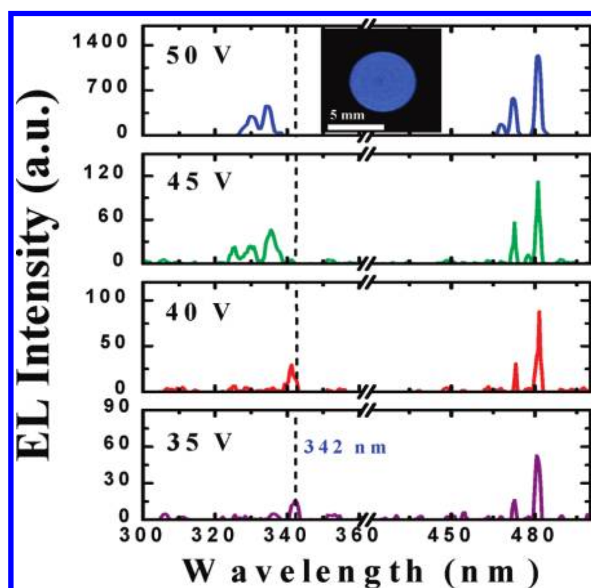

FIGURE 6. EL spectra recorded from the p-n ZnO NW arrays under various operating voltage conditions in room temperature. The top view photograph of the bright light emitting spot at 50 V is displayed in the inset figure. The vertical dash lines located at 342 nm are introduced as the guide to the eye.

voltage of 50 V is displayed as an inset in Figure 6. In the low operating voltage regime, only the typical near-band edge emission at ~385 nm and the DL emission at ~560 nm can be observed (Supporting Information Figure S6). As the operating voltage further increases, the bright light emission from ZnO NW p-n homojunctions at 35 V was distinctively observed with the UV light emission at 342 nm and the DL emissions comprising some distinguishable emitting peaks around 480 nm. Further, as the operating voltage was increased from 35 to 50 V, the short-wavelength UV emission and the DL light emissions spectra exhibiting the multiple emitting peaks accompanied with the appearance of additional peaks can be observed. On the basis of the comparison between the CL and EL spectra, it is suggested that the light emission at high voltage regime would take place at the n-type ZnO segment. In addition, the high brightness light emission from p-n ZnO homojunctions can also be observed after four months following device fabrication, revealing the high stability of our LED devices in ambient.

Importantly, we found that there were the fine structures comprising multiple peaks with the specific energies exhibited in the DL emission spectra, as presented in Supporting Information Figure S7. By comparing the DL spectra to the PL spectra recorded from the as-grown n-type ZnO:Zn NWs, it reveals that the spectral structures of the DL emitting peaks exhibit a similar fine structures to that of the PL spectra at room temperature (Supporting Information Figure S8). Furthermore, the fine structures with phonon replicas observed in the PL spectra were reported previously in high-quality ZnO films[36,37] and nanorods/nanowires.[38,39] The fine structure in PL spectrum recorded from the ZnO:Zn nanorods reported previously,[38] which suggested that the fine structure can be attributed to the longitudinal optical (LO) phonon-assisted emission, is similar to that measured from our samples. The mechanism for light emission with a narrow width in DL spectra at room temperature is yet to be clarified. Further investigation will be necessary to find out the physical mechanism of the narrow-width fine structures observed in the DL emission spectra.

For the UV light emission spectra, the 342 nm UV light emission can be contributed by the BM effect as discussed in a previous paragraph related to part of Figure 4. As the operating voltage increasing from 35 to 45 V, the blue-shift effect in the UV light emission spectra would be evident for the light wavelength shifted from 342 to 325 nm. A slight light emission degradation in EL spectrum for device operated at 50 V can be observed, which is probably due to the electrical heating at p-n NWs in high operating voltage regime. Note that as the operating voltage further increases, the increment of the magnitude of the electrical field within the transition region, which would result in the increment of the extra energies in the hole carriers, may cause the blue shift in the UV light emission spectra from 342 to 325 nm. The band diagram of p-n ZnO NW under the equilibrium condition and the high voltage condition are illustrated in Figure 7. We believe that the hole carriers cannot successfully arrive at the n-type region without this narrow transition

© XXXX American Chemical Society

DOI: 10.1021/nl101907h | Nano Lett. XXXX, xxx, 000–000

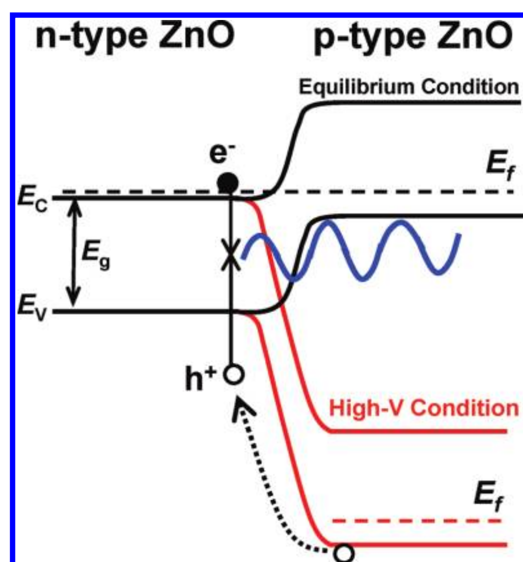

FIGURE 7. Energy band diagram of p-n homojunction under the equilibrium condition and the high operating voltage condition. E_g is the bandgap of ZnO, E_f is Fermi level and E_c and E_v are the conduction band and valence band of NW, respectively.

region before it recombined with electrons to generate the light emission; hence, the holes can easily pass through such a narrow transition region and then recombine with electrons at n-type region to generate the UV light emission above bandgap energy.

In conclusion, catalyst-free p-n ZnO NW arrays were epitaxially synthesized by utilizing the in situ doping process. The width of doping transition region in this p-n homojunctions can be scaled down to sub-50 nm along the [0001] ZnO NW growth direction. The observation of CL emission peak at 340 nm from n-type ZnO:Zn NWs is presumably due to the Burstein−Moss effect in the high electron carrier concentration regime. Moreover, the blue shift in UV light emission for wavelength from 342 to 325 nm occurred with increasing operating voltage. As a result, in situ doping engineering in the synthesis of the ZnO NW p-n homojunctions is a promising strategy to create the building blocks for short-wavelength UV LEDs and photoelectronics applications.

Acknowledgment. The authors would like to thanks C. T. Hsu for technical assistance. This research was supported by the Republic of China National Science Council through Grant NSC 97-2120-M-007-003.

Supporting Information Available. This material is available free of charge via the Internet at http://pubs.acs.org.

REFERENCES AND NOTES

(1) Sandhu, A. *Nat. Photonics* **2007**, *1*, 38.
(2) Huang, M. H.; Mao, S.; Feick, H.; Yan, H.; Wu, Y.; Hannes, Kind.; Weber, E.; Russo, R.; Yang, P. *Science* **2001**, *292*, 1897.
(3) Kinoshita, A.; Hirayama, H.; Ainoya, M.; Aoyagi, Y.; Hirata, A. *Appl. Phys. Lett.* **2000**, *77*, 175.
(4) Koizumi, S.; Watanabe, K.; Hasegawa, M.; Kanda, H. *Science* **2001**, *292*, 1899.
(5) Watanabe, K.; Taniguchi, T.; Kanda, H. *Nat. Mater.* **2004**, *3*, 404.
(6) Lim, J. H.; Kang, C. K.; Kim, K. K.; Park, I. K.; Hwang, D. K.; Park, S. J. *Adv. Mater.* **2006**, *18*, 2720.
(7) Zhong, Z.; Qian, F.; Wang, D.; Lieber, C. M. *Nano Lett.* **2003**, *3*, 343.
(8) Lee, S. K.; Kim, T. H.; Lee, S. Y.; Choi, K. C.; Yang, P. *Philos. Mag.* **2007**, *87*, 2105.
(9) Zhang, X. M.; Lu, M. Y.; Zhang, Y.; Chen, L. J.; Wang, Z. L. *Adv. Mater.* **2009**, *21*, 2767–2770.
(10) Sun, J. C.; Zhao, J. Z.; Liang, H. W.; Bian, J. M.; Hu, L. Z.; Zhang, H. Q.; Liang, X. P.; Liu, W. F.; Du, G. T. *Appl. Phys. Lett.* **2007**, *90*, 121128.
(11) Chu, S.; Lim, J. H.; Mandalapu, L. J.; Yang, Z.; Li, L.; Liu, J. L. *Appl. Phys. Lett.* **2008**, *92*, 152103.
(12) Park, C. H.; Zhang, S. B.; Wei, S. H. *Phys. Rev. B* **2002**, *66*, No. 073202.
(13) Lee, W. J.; Kang, J.; Chang, K. J. *Phys. Rev. B* **2006**, *73*, No. 024117.
(14) Yang, Y.; Sun, X. W.; Tay, B. K.; You, G. F.; Tan, S. T.; Teo, K. L. *Appl. Phys. Lett.* **2008**, *93*, 253107.
(15) Zhang, J. Y.; Li, P. J.; Sun, H.; Shen, X.; Deng, T. S.; Zhu, K. T.; Zhang, Q. F.; Wu, J. L. *Appl. Phys. Lett.* **2008**, *93*, No. 021116.
(16) Sun, X. W.; Ling, B.; Zhao, J. L.; Tan, S. T.; Yang, Y.; Shen, Y. Q.; Dong, Z. L.; Li, X. C. *Appl. Phys. Lett.* **2009**, *95*, 133124.
(17) Pan, Z. W.; Dai, Z. R.; Wang, Z. L. *Science* **2001**, *291*, 1947.
(18) Dai, Z. R.; Pan, Z. W.; Wang, Z. L. *Adv. Funct. Mater.* **2003**, *13*, 9.
(19) Xiang, B.; Wang, P.; Zhang, X.; Dayeh, S. A.; Aplin, D. P. R.; Soci, C.; Yu, D.; Wang, D. *Nano Lett.* **2007**, *7*, 323.
(20) Lu, M. P.; Song, J.; Lu, M. Y.; Chen, M. T.; Gao, Y.; Chen, L. J.; Wang, Z. L. *Nano Lett.* **2009**, *9*, 1223.
(21) Wang, Z. L.; Song, J. H. *Science* **2006**, *312*, 242.
(22) Lin, S. S.; Hong, J. I.; Song, J. H.; Zhu, Y.; He, H. P.; Xu, Z.; Wei, Y. G.; Ding, Y.; Snyder, R. L.; Wang, Z. L. *Nano Lett.* **2009**, *9*, 3877.
(23) Lin, S. S.; Song, J. H.; Lu, Y. F.; Wang, Z. L. *Nanotechnology* **2009**, *20*, 365703.
(24) Hong, W. K.; Sohn, J. I.; Hwang, S. S.; Jo, G.; Song, S.; Kim, S. M.; Ko, H. J.; Park, S. J.; Welland, M. E.; Lee, T. *Nano Lett.* **2008**, *8*, 950.
(25) Vanheusden, K.; Seager, C. H.; Warren, W. L.; Tallant, D. R.; Voigt, J. A. *Appl. Phys. Lett.* **1996**, *68*, 403.
(26) Pan, N.; Wang, X.; Li, M.; Li, F.; Hou, J. G. *J. Phys. Chem. C* **2007**, *111*, 17265.
(27) Xue, H.; Pan, N.; Zeng, R.; Li, M.; Sun, X.; Ding, Z.; Wang, X.; Hou, J. G. *J. Phys. Chem. C* **2009**, *113*, 12715.
(28) (a) Chang, Y. C.; Chen, L. J. *J. Phys. Chem. C* **2007**, *111*, 1268. (b) Chang, Y. C.; Tang, W. C.; Chang, C. M.; Hsu, P. C.; Chen, L. J. *Cryst. Growth Des.* **2009**, *9*, 3161. (c) Chang, Y. C.; Wu, H. W.; Chen, H. L.; Wang, W. Y.; Chen, L. J. *J. Phys. Chem. C* **2009**, *113*, 14778.
(29) Yin, M.; Gu, Y.; Kuskovsky, I. L.; Andelman, T.; Zhu, Y.; Neumark, G. F.; O'Brien, S. *J. Am. Chem. Soc.* **2004**, *126*, 6206.
(30) Baranov, A. N.; Panin, G. N.; Kang, T. W.; Oh, Y. J. *Nanotechnology* **2005**, *16*, 1918.
(31) Fonoberov, V. A.; Balandin, A. A. *Phys. Rev. B* **2004**, *70*, 195410.
(32) Combescot, M.; Combescot, R.; Roulet, B. *Eur. Phys. J. B* **2001**, *23*, 139.
(33) Sakai, K.; Kakeno, T.; Ikari, T.; Shirakata, S.; Sakemi, T.; Awai, K.; Yamamoto, T. *J. Appl. Phys.* **2006**, *99*, No. 043508.
(34) Sernelius, B. E.; Berggren, K. F.; Jin, Z. C.; Hamberg, I.; Granqvist, C. G. *Phys. Rev. B* **1988**, *37*, 10244.
(35) Hagemark, K. I. *J. Solid State Chem.* **1976**, *16*, 293.
(36) Reynolds, D. C.; Look, D. C.; Jogai, B. *J. Appl. Phys.* **2001**, *89*, 6189.
(37) Shan, W.; Walukiewicz, W.; Ager III, J. W.; Yu, K. M.; Yuan, H. B.; Xin, H. P.; Cantwell, G.; Song, J. J. *Appl. Phys. Lett.* **2005**, *86*, 191911.
(38) Patra, M. K.; Manzoor, K.; Manoth, M.; Vadera, S. R.; Kumar, N. *J. Lumin.* **2008**, *128*, 267.
(39) Zimmler, M. A.; Voss, T.; Ronning, C.; Capasso, F. *Appl. Phys. Lett.* **2009**, *94*, 241120.

© XXXX American Chemical Society

DOI: 10.1021/nl101907h | *Nano Lett.* **XXXX,** *xxx,* 000–-000